Rev. Roum. Sci. Techn.– Électrotechn. et Énerg.
Vol. 71, 3, pp. 349–354, Bucarest, 2026

EVALUATION OF METAHEURISTIC TRACKING METHODS IN PHOTOVOLTAIC WATER PUMPING UNDER PARTIAL SHADING

AHMED MERBAH[1], SID AHMED TADJER[1]

Keywords: Photovoltaic (PV); Water pumping; Particle swarm optimization (PSO); Grey wolf optimization (GWO); Marine predator algorithm (MPA).

The use of photovoltaic (PV) energy for water pumping is one of the most promising applications of renewable energy systems. This paper proposes advanced maximum power point tracking (MPPT) techniques to improve the performance of PV-based water-pumping systems under partial shading conditions. The proposed system consists of a PV generator, a DC–DC converter, and a brushless DC (BLDC) motor-driven water pump. Conventional MPPT techniques, such as Perturb and Observe (P&O), fail to track the global maximum power point (GMPP) under partial shading conditions. Therefore, particle swarm optimization (PSO), grey wolf optimization (GWO), and marine predator algorithm (MPA)-based approaches are investigated to ensure effective global maximum power point tracking (GMPPT). The proposed methods are evaluated in MATLAB/Simulink across various partial-shading scenarios. The results demonstrate improved tracking performance compared with the conventional P&O method and provide a comparative assessment of the investigated metaheuristic techniques in terms of convergence behavior and steady-state performance.

1. INTRODUCTION

The demand for traditional energy sources continues to grow worldwide. It is important to note, however, that although these resources are economical, efficient, and easily transportable, their increasing scarcity is gradually harming the ecosystem [1]. Renewable energy sources, especially solar power, offer a promising alternative. Many countries are making substantial investments to balance energy production and consumption while maintaining ecological sustainability [2]. Solar-powered water pumping systems in rural and developing areas can serve as a superior alternative to conventional systems [3]. Since these systems rely on solar power, the photovoltaic (PV) output is primarily influenced by insolation, load characteristics, and temperature [4]. To ensure the optimal performance of PV systems, implementing maximum power point tracking (MPPT) strategies is essential for extracting the maximum available power [5]. Among the various MPPT algorithms, the perturb-and-observe (P&O) method is among the most widely used due to its simplicity and effectiveness [6]. However, under partial shading conditions (PSCs), the output power of PV systems can be significantly reduced when conventional algorithms fail to accurately track the global maximum power point (GMPP) [20]. In such conditions, the power–voltage characteristics of PV modules become multimodal, exhibiting multiple local power peaks [7]. To overcome MPPT challenges in PSCs, researchers have developed several bio-inspired optimization techniques, a class of soft computing methods known as metaheuristic algorithms [12]. These bio-inspired algorithms include particle swarm optimization (PSO) [8], grey wolf optimization (GWO) [9], and the marine predator algorithm (MPA) [10]. These algorithms can effectively identify the GMPP with high accuracy even in the presence of multiple local maxima, while significantly reducing steady-state oscillations [11].

Despite their ability to locate the global maximum power point under partial shading conditions, metaheuristic MPPT algorithms exhibit different dynamic behaviors in terms of convergence speed, tracking accuracy, and steady-state oscillations. The balance between exploration and exploitation mechanisms directly affects the convergence time and the quality of the final operating point. Recent comparative studies have shown that some algorithms achieve faster convergence, whereas others offer improved tracking accuracy and reduced steady-state fluctuations, highlighting the importance of selecting the most suitable optimization technique for the application requirements and operating conditions [21,22].

This study presents a PV-powered water-pumping system incorporating a DC–DC boost converter, a voltage-source inverter (VSI), and a BLDC motor under partial shading conditions. The study highlights the limitations of conventional MPPT techniques in tracking the global maximum power point (GMPP). In addition, advanced optimization-based approaches are investigated by analyzing their effects on harvested power, rotor speed, electromagnetic torque, and overall system efficiency to identify the most reliable and efficient solution for sustainable PV water pumping applications.

2. DESIGN OF THE SYSTEM

The SPV array powers the motor–pump system via a boost converter and a voltage-source inverter (VSI), which generates the required electronic switching signals. Rotor position is detected using Hall sensors that provide three signals every 60°. These signals are converted into six switching pulses to drive the inverter [14], as illustrated in Table 1. The boost converter regulates the SPV output using the MPPT controller, which adjusts the IGBT duty cycle to ensure maximum power extraction. As shown in Fig. 1, the VSI converts the reDC power into AC power to drive a BLDC motor mechanically coupled to a centrifugal pump.

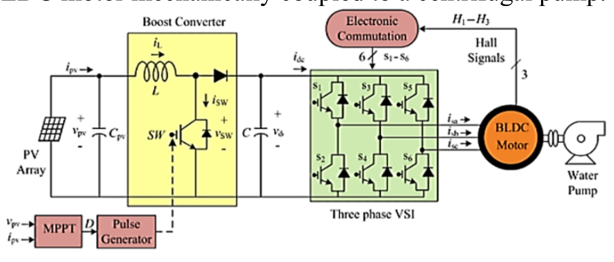

Fig. 1 – PV-powered water pumping system configuration.

Table 1

Switching states of VSI for each set of Hall-Effect signal states.

Hall signals				Switching states					
θ, deg	H_3	H_2	H_1	T_1	T_2	T_3	T_4	T_5	T_6
NA	0	0	0	0	0	0	0	0	0
0–60	1	0	1	1	0	0	1	0	0
60–120	0	0	1	1	0	0	0	0	1
120–180	0	1	1	0	0	1	0	0	1
180–240	0	1	0	0	1	1	0	0	0
240–300	1	1	0	0	1	0	0	1	0
300–360	1	0	0	0	0	0	1	1	0
NA	1	1	1	0	0	0	0	0	0

[1]Department of Automation and Process Electrification, University M'Hamed Bougara, 35000, Boumerdes, Algeria.
E-mail : a.merbah@univ-boumerdes.dz, s.tadjer@univ-boumerdes.dz

DOI: 10.59277/RRST-EE.2026.3.2

4. MAXIMUM POWER POINT TRACKING

The performance of an MPPT technique is assessed by its complexity, cost, tracking speed, accuracy, and sensor requirements [15]. Among them, the P&O method is the most used, adjusting module voltage to evaluate power variation [16]. However, partial shading (PS), caused by dust, damage, or moving clouds, reduces PV efficiency. To address this, bypass diodes and advanced MPPT metaheuristic algorithms have been introduced. These algorithms, inspired by nature, optimize complex problems beyond traditional methods through local/global searches and cooperative mechanisms [13].

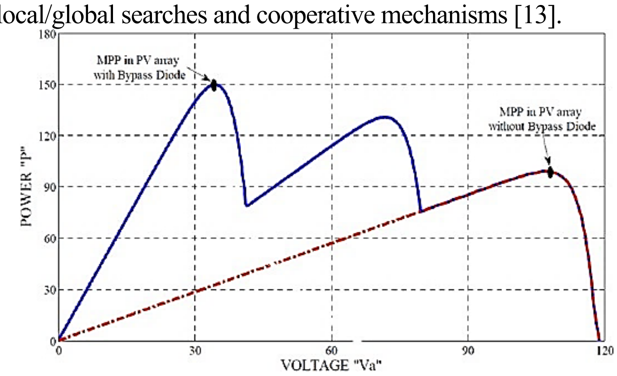

Fig. 3 – PV characteristic curves under partial shading

3.1. PARTICLE SWARM OPTIMIZATION

In basic terms, this algorithm uses the concept of swarm intelligence. Particles navigate through a multidimensional search space. Each particle adjusts its position according to its own experience (P_{est}), and that of its neighbors (G_{uest}). The swarm, or the group of particles, is guided by these historical optimal positions [8].

$$\mathbf{V}_i^{k+1}=\mathrm{w}\mathbf{V}_i^{k}+\mathrm{c}_1\mathrm{r}_1\left(\mathrm{P}^k_{\mathrm{best}i}-\mathbf{V}_i^k\right)+\mathrm{c}_2\mathrm{r}_2\left(\mathrm{G}^k_{\mathrm{best}i}-\mathbf{X}_i^k\right), \tag{1}$$

$$\mathbf{X}_i^{k+1}=\mathbf{X}_i^{k}+\mathbf{V}_\mathrm{i}^{+1}, \tag{2}$$

$$P_{best_i}=\begin{cases} P_{best_i} & f(x)\geq f(P_i) \\ \mathbf{X}_i & f(x)\leq f(P_i) \end{cases} \tag{3}$$

$G_{best}=\{f(P_{best_0});f(P_{best_1});\ldots;f(P_{best_m})\}$, $i = 1,2,\ldots,m$, m is the number of particles, k is the iteration count, Xi and Vi are the position and velocity, w is the inertia weight, c_1 and c_2 are control parameters, and r_1 and r_2 are random values in (0,1). P_{est} and G_{best} are the personal and global bests, respectively Fig. 4.

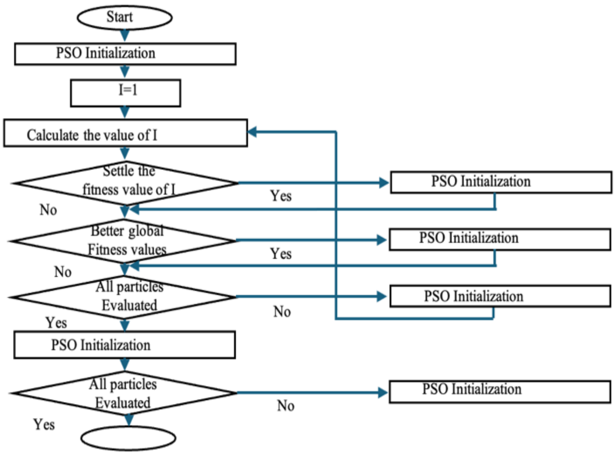

Fig. 2 – Flow chart for PSO algorithm.

3.2. GREY WOLF OPTIMIZATION

Grey wolves, apex predators living in packs of 5–12 with a defined social hierarchy, exhibit encircling hunting behavior mathematically modeled by the following equations [9]:

$$\vec{\mathbf{V}}=\left|\vec{\mathrm{C}}\cdot\vec{\mathbf{X}}_P(t)-\vec{\mathbf{X}}_P(t)\right|, \tag{4}$$

$$\vec{\mathbf{X}}(t+1)=\vec{\mathbf{X}}_\mathrm{p}(t)-\vec{\mathbf{A}}\cdot\vec{\mathbf{V}}, \tag{5}$$

where t denotes the current iteration. $\vec{\mathbf{V}},\vec{\mathbf{A}}$ and $\vec{\mathbf{C}}$ denote coefficient vectors, $\vec{\mathbf{X}}_\mathbf{P}$ is the position vector of the prey, and $\vec{\mathbf{X}}$ indicates the position of the grey wolf.

$$\vec{\mathbf{A}}=\vec{\mathbf{a}}(2\vec{\mathbf{r}}_1-1),\ \vec{\mathbf{C}}=2\vec{\mathbf{r}}_2, \tag{6}$$

where, $\vec{\mathbf{r}}_1$, $\vec{\mathbf{r}}_2$ random vectors in [0,1] and components $\vec{\mathbf{A}}$ are linearly decreased from 2 to 0 over the iterations. Alpha (α), Beta (β) and Delta (δ) wolves guide other agents (**Ω**) toward prey the estimated position [9]. The formulas are as follows:

$$\vec{\mathbf{X}}_1=\left(\vec{\mathbf{X}}_\alpha-\vec{\mathbf{A}}_1.(\vec{\mathbf{D}}_\alpha)\right),\ \vec{\mathbf{X}}_2=\left(\vec{\mathbf{X}}_\beta-\vec{\mathbf{A}}_2.(\vec{\mathbf{D}}_\beta)\right),\vec{\mathbf{X}}_3=\left(\vec{\mathbf{X}}_\delta-\vec{\mathbf{A}}_3.(\vec{\mathbf{D}}_\delta)\right) \tag{7}$$

$$\vec{\mathbf{X}}(t+1)=\frac{\vec{\mathbf{X}}_1+\vec{\mathbf{X}}_2+\vec{\mathbf{X}}_3}{3}. \tag{8}$$

Each grey wolf updates its position using the averaged influence of Alpha (α), Beta (β), and Delta (δ) wolves, as shown in eq. (8) and illustrated in Fig. 4.

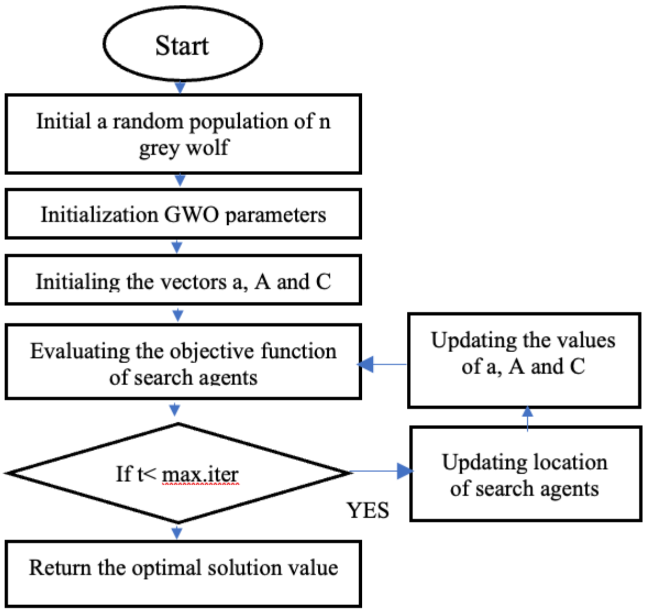

Fig. 4 – Flowchart for GWO MPPT algorithm.

3.3. MARINE PREDATOR ALGORITHM

MPA is a nature-inspired metaheuristic optimization method based on predator foraging behavior [18], where Lévy motion models exploration in prey-scarce environments and Brownian motion governs search in prey-abundant conditions [17],

$$\mathrm{levy}(\alpha) = 0.05\times\frac{\mathbf{x}}{|y|^{\frac{1}{\alpha}}}, \tag{9}$$

$$f(x,\mu,\sigma)=\frac{1}{\sqrt{2\pi}}\mathrm{e}^{\frac{-x^2}{2}}. \tag{10}$$

The high-speed ratio stage, when Iter < 1/3Max_Iter. The optimal approach for the predator is to remain stationary, whereas the prey's movement follows Brownian motion [10].

$$\overrightarrow{\mathbf{stepsize}_\alpha}=\overrightarrow{\mathbf{R}_\beta}\otimes\left(\overrightarrow{\mathbf{Elite}_\alpha}-\overrightarrow{\mathbf{R}_\beta}\otimes\overrightarrow{\mathrm{Prey}_\alpha}\right);\ \alpha=1\ldots n \qquad (11)$$

$$\overrightarrow{\mathbf{Prey}_\alpha}=\overrightarrow{\mathbf{Prey}_\alpha}+P\,\overrightarrow{\mathbf{R}}\otimes\left(\overrightarrow{\mathbf{Stepsize}_\alpha}\right), \qquad (12)$$

where, P = 0.5, R is a uniform random vector in [0, 1], and RB is a Brownian-based random value vector.

The second phase, termed unit velocity ratio, occurs when predator and prey move at equal speed. Positioned mid-iteration as mathematically formulated as,

$$\overrightarrow{\mathbf{stepsize}_\alpha}=\overrightarrow{\mathbf{R}_\mathrm{L}}\otimes\left(\overrightarrow{\mathbf{Elite}_\alpha}-\overrightarrow{\mathbf{R}_\mathrm{L}}\otimes\overrightarrow{\mathbf{Prey}_\alpha}\right);\ \alpha=1,\ldots,\frac{n}{2}, \qquad (13)$$

$$\overrightarrow{\mathbf{Prey}_\alpha}=\overrightarrow{\mathbf{Prey}_\alpha}+P\,\overrightarrow{\mathbf{R}}\otimes\overrightarrow{\mathbf{stepsize}_\alpha}, \qquad (14)$$

R_L is a random number based on the Levy distribution. Step size in Levy distribution. For the second half of the population:

$$\overrightarrow{\mathbf{stepsize}_\alpha}=\overrightarrow{\mathbf{R}_\mathrm{B}}\otimes\left(\overrightarrow{\mathbf{R}_\mathrm{B}}\otimes\overrightarrow{\mathbf{Elite}_\alpha}-\overrightarrow{\mathbf{Prey}_\alpha}\right);\ \alpha=\frac{n}{2},..,n \qquad (15)$$

$$\overrightarrow{\mathbf{Prey}_\alpha}=\overrightarrow{\mathbf{Elite}_\alpha}+P\ \mathrm{CF}\otimes\overrightarrow{\mathbf{stepsize}_\alpha}. \qquad (16)$$

Here, represents an adaptive parameter for controlling the predator's step size [19] low-velocity ratio at this point. The best strategy for predators is the Lévy flight campaign. This phase is denoted as:

$$\overrightarrow{\mathbf{stepsize}_\alpha}=\overrightarrow{\mathbf{R}_\mathrm{L}}\otimes\left(\overrightarrow{\mathbf{R}_\mathrm{L}}\otimes\overrightarrow{\mathbf{Elite}_\alpha}-\overrightarrow{\mathbf{Prey}_\alpha}\right);\ \alpha=1,\ldots n. \qquad (17)$$

The flowchart below illustrates the three stages of MPA:

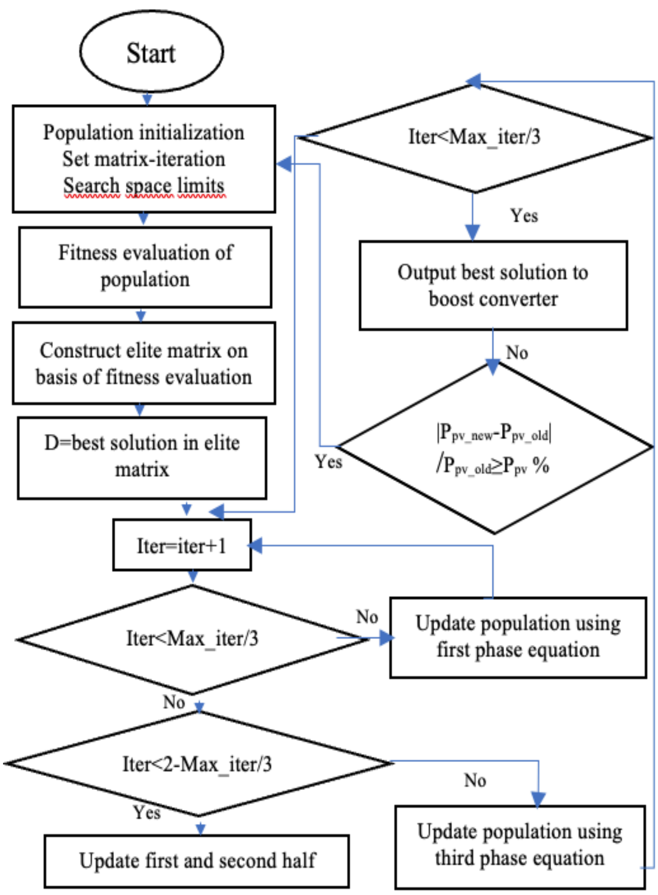

Fig. 5 – Flowchart for MPA algorithm.

4. SIMULATION AND RESULTS

4.1. UNDER NORMAL CONDITIONS

The proposed system is simulated using MATLAB/Simulink 2021a. The PV module used in the simulation is the Zhejiang Sunflower Light Energy Science Technology SF125×125-72-M-175W. The system consists of a 1350 W BLDC motor operating at 230 V, connected to a 1574 W PV array with a maximum voltage and current of 107 V and 14.7 A, respectively. The PV array is subjected to rapidly varying solar irradiance levels, ranging from 1000 to 700 W/m² at 25°C, for a (3P×3S) string configuration. Figure 6 presents the corresponding P–V characteristic.

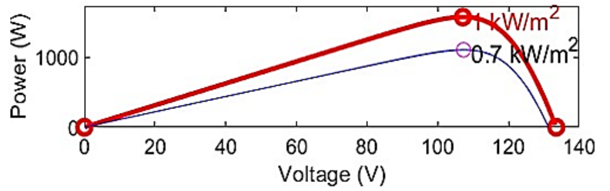

Fig. 6 – P-V characteristics under uniform conditions.

The P&O algorithm is simulated, showing the PV output and the rotor speed under varying irradiance in Fig. 8 (a).

4.2. UNDER PARTIAL SHADING

Under non-uniform shading conditions, the PV array exhibits multiple local maximum power points (LMMPs) on the P–V characteristic curves for all investigated scenarios (S1: [1000, 700, 300], S2: [800, 500, 200], and S3: [900, 600, 200]). in each case, a unique global maximum power point corresponds to the highest peak. the obtained gmpp values are 784 W for S1, 565 W for S2, and 675 W for S3, as illustrated in Fig. 7.

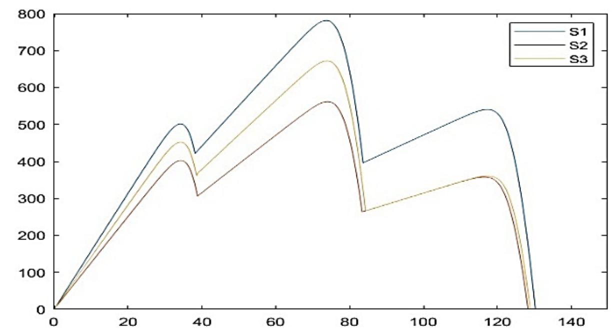

Fig. 7 – P-V characteristics under partial shading conditions.

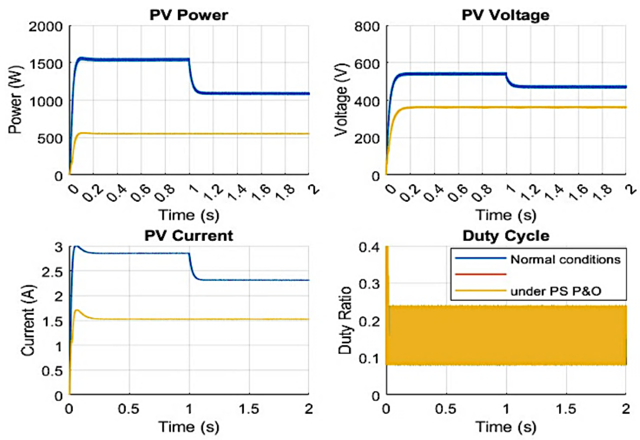

Fig. 8 – Dynamic performance of the PV system based on the P&O MPPT algorithm under varying irradiance and partial shading conditions.

As shown in Fig.8 the PV power, voltage, and current closely follow the irradiance curves, with the P&O algorithm achieving 1570 W under STC, demonstrating rapid MPP convergence and a smooth motor response. However, under PS conditions, the P&O algorithm fails to track the GMPP. To address this issue, a simulation is conducted for the three PS scenarios, illustrating the performance of each method. PSO employs a population size of N = 3 and T = 10 iterations with parameters c1 = 1.2, and c2 = 2 given results in Fig. 9.

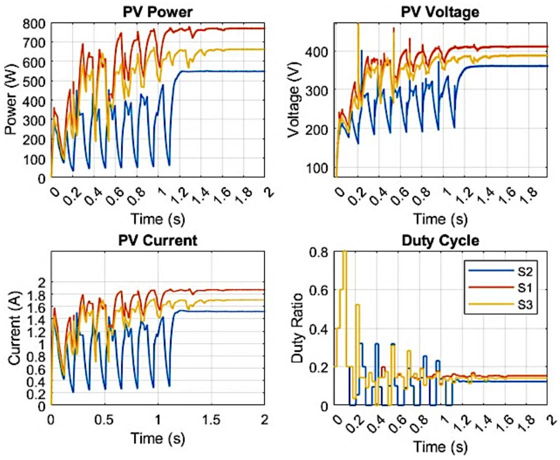

Fig. 9 – Dynamic PV performance of the proposed system under PS conditions using PSO for the three scenarios.

Initially, the PV variables exhibit transient oscillations during the PSO search. The system reaches steady-state operation at approximately 1.4 s, achieving output powers of 772.5 W, 550 W, and 663 W for Scenarios 1–3, respectively, confirming successful GMPP tracking. Under the same operating conditions, the GWO algorithm is evaluated using $N = 4$wolves and $T = 200$iterations with a linearly decreasing control parameter, as illustrated in Fig. 10.

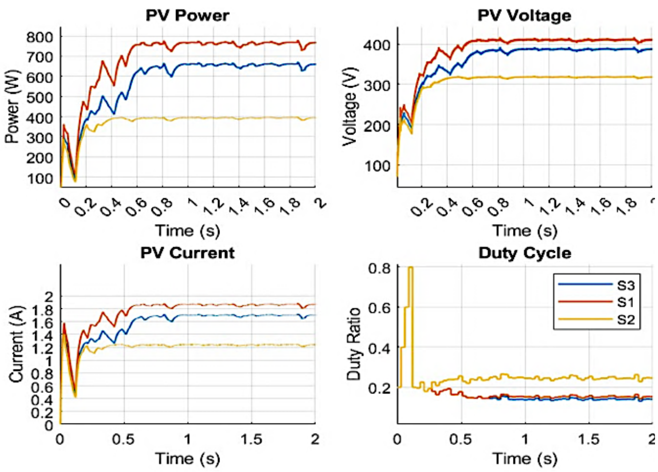

Fig. 10 – Dynamic PV performance of the proposed system under PS conditions using GWO for the three scenarios.

As shown in Fig. 10, the PV variables experience transient fluctuations during the GWO search process before reaching steady state between 0.6 s and 0.8 s. The algorithm successfully tracks the GMPP in scenarios 1 and 3, achieving output powers of 774.5 W and 662 W, respectively. However, in scenario 2, it converges to a local optimum (395 w) due to the limited number of iterations. To further assess the MPPT techniques investigated, the marine predator algorithm (MPA) is evaluated using $N = 4$ agents, $T =$ 10 iterations, $FADs = 0.2$, $P = 0.5$, and a Lévy exponent $\beta = 1.5$, with the duty cycle constrained to the range $[0, 1]$. The corresponding results are presented in Fig. 11.

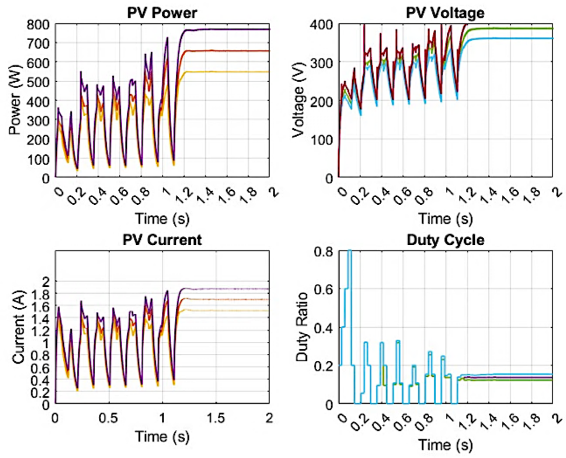

Fig. 11 – Dynamic PV performance of the proposed system under PS conditions using MPA for the three scenarios.

In terms of convergence time, all parameters exhibit rapid transient oscillations before stabilizing at approximately 1.23 s, with no noticeable steady-state oscillations. Moreover, the PV power reaches steady-state values of 772.3 W, 552 W, and 664 W, thereby improving rotor speed and load torque performance across the three scenarios. These results improve the MPA's effectiveness in accurately tracking the GMPP.

Figure 12 illustrates the relationship between MPPT performance, rotor speed, and the power delivered to the BLDC motor under the investigated operating conditions.

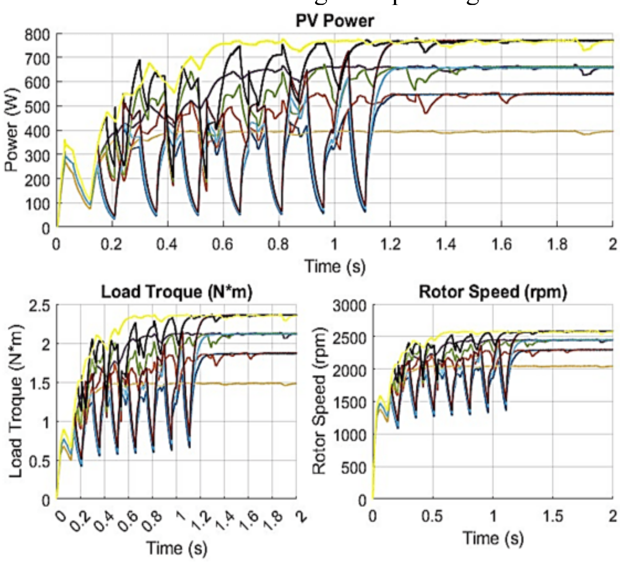

Fig. 12 – Combined power, load torque, and rotor speed of the used algorithms under partial shading (three scenarios).

Figure 12 shows that the PSO, GWO, and MPA algorithms successfully tracked the GMPP under partial shading, whereas P&O stagnated at a local MPP. PSO reached high power but suffered from steady-state noise; GWO achieved near-optimal tracking with moderate oscillations and failed in the second scenario; while MPA offered the best trade-off with fast convergence, minimal noise, and stable rotor speed.

To improve the robustness and repeatability of the proposed approach shown in Fig. 12, each scenario was tested across 35 independent runs. Statistical metrics, including the mean and variance of convergence time, tracking efficiency, and steady-state ripple, were analyzed, as summarized in Table 2.

Table 2

Comparative analysis of MPPT used algorithms for all PS cases.

Scenario	Mean time (s)	Variance time (s²)	Mean power (W)	Variance power	efficiency (%)	Ripple (%)
S1 (PSO)	1.394	$2.96\text{x}10^{-5}$	772.5	0.15	98.52	0.12
S2 (PSO)	1.277	$1.56\text{x}10^{-4}$	550.6	1.74	97.45	0.51
S3 (PSO)	1.457	$2.89\text{x}10^{-4}$	656.5	0.95	97.25	0.34
S1 (GWO)	0.646	$5.89\text{x}10^{-4}$	772.2	3.61	98.49	0.18
S2 (GWO)	0.420	$4.00\text{x}10^{-4}$	394.7	3.63	69.85	1.12
S3 (GWO)	0.743	$9.33\text{x}10^{-4}$	660,0	4.00	97.78	0.41
S1 (MPA)	1.23	$4.00\text{x}10^{-6}$	772.7	0.49	98.55	0.15
S2 (MPA)	1.235	$2.50\text{x}10^{-5}$	550.6	1.72	97.50	0.74
S3 (MPA)	1.235	$4.00\text{x}10^{-6}$	659.8	2.80	97.75	0.28

Table 2 presents the statistical comparison of the investigated MPPT techniques under different partial shading scenarios. The obtained results indicate that PSO and MPA achieve high tracking efficiency and stable steady-state performance in all scenarios. Although GWO converges faster, it fails to track the global maximum power point in Scenario 2, resulting in reduced tracking efficiency. Furthermore, MPA demonstrates the lowest convergence-time variance, confirming its robustness and repeatability under varying operating conditions.

Furthermore, additional analyses were conducted during the transient period for all scenarios, including tracking efficiency, harvested energy, and power delivered to the motor shaft, as expressed by the following equation, and DC-link voltage ripple, as presented in Table 3.

Table 3

Comparative analysis of the performance of the MPPT algorithms used during the transient window for all PS cases.

Scenario	Harvested Energy (J)	DC-Link Ripple voltage	Efficiency (%)	Delivered Power(W)
S1(PSO)	1523.26	0.015	64.77	633.1
S1(GWO)	1635.24	0.025	69.53	636.5
S1(MPA)	2332.41	0.020	99.17	635.7
S2(PSO)	1348.77	0.014	79.57	541.6
S2(GWO)	1080.82	0.013	63.77	542.4
S2(MPA)	1674.93	0.015	98.82	541.0
S3(PSO)	1616.32	0.018	80.18	449.2
S3(GWO)	1635.24	0.030	81.11	317.6
S3(MPA)	2001.55	0.022	99.28	449.8

Table 3 presents the transient performance of the investigated MPPT methods under the three partial-shading scenarios. The PSO method exhibits moderate tracking capability with acceptable harvested energy and efficiency across all scenarios. The proposed MPA approach maintains the best overall performance, achieving the highest harvested energy and MPPT efficiency in all cases, which confirms its robust and stable convergence toward the GMPP under varying shading conditions. In contrast, the GWO method shows inconsistent behavior and fails to maintain reliable tracking performance in Scenario S2, resulting in reduced harvested energy and lower efficiency compared with the other methods

5. **CONCLUSION**

In conclusion, the comparative analysis under the three partial shading scenarios confirms that the MPPT technique significantly affects both the electrical and mechanical performance of the PV-driven motor system. The conventional P&O method exhibits higher oscillations and lower tracking capability under changing irradiance conditions, resulting in reduced extracted power and lower mechanical power delivery. PSO improves the tracking response and system stability compared with P&O, while GWO shows inconsistent behavior and fails to ensure reliable GMPP tracking in Scenario S2. In contrast, the proposed MPA-based MPPT method consistently achieves the highest tracking efficiency and harvested energy in all scenarios, while providing stable DC-link performance and improved power delivery to the motor shaft. Since the developed mechanical power is proportional to the rotor speed and load torque.

For future work, experimental validation or hardware-in-the-loop (HIL) implementation is required to further substantiate the simulation results and confirm the practical applicability of the proposed approach. This will also enable a more realistic assessment of implementation challenges such as sensor noise, duty-cycle saturation, converter non-idealities, switching losses, and rapidly changing partial shading conditions.

CREDIT AUTHORSHIP CONTRIBUTION

TADJER SID AHMED: Presented the idea.
MERBAH AHMED: Theory and simulation, Results analysis, data, and design methodology.

Received on 25 September 2025

APPENDIX

The bypass diode parameters used in the simulations are:

- Forward voltage $V_f = 0.8$V
- On-state resistance $R_{on} = 0.001\ \Omega$
- Snubber resistance $R_s = 500\ \Omega$
- Snubber capacitance $C_s = 250 \times 10^{-9}$F

REFERENCES

1. H. Abed, S. Bouri, H. Benariba, “Comparison between several methods of identification of photovoltaic parameters”, Rev. Roum. Sci. Techn. – Électrotechn. et Énerg., **70**, *4*, pp. 489–494 (2025).
2. C.J. Ejiyi, D. Cai, D. Thomas et al., “Comprehensive review of artificial intelligence applications in renewable energy systems: current implementations and emerging trends”, Journal of Big Data, **12**, Article 169 (2025).
3. A. Bartram, J. Smith, “External support for solar-powered water pumping systems in rural areas: a systematic review”, Environmental Science & Technology, **58**, *41*, pp. 18053–18063 (2024).
4. M. Qureshi et al., “A novel adaptive control approach for maximum power point tracking in photovoltaic systems”, Energies, **16**, *6*, Article 2782 (2023).
5. L. Khettache, M.R. Rezoug, A. Saadi, L. Sahraoui, “A novel design of a photovoltaic system based on a linear induction motor and reciprocating pump”, Rev. Roum. Sci. Techn. – Électrotechn. et Énerg., **70**, *1*, pp. 3–8 (2025).
6. A. Zouhri, “Advanced perturb and observe algorithm for maximum power point tracking in photovoltaic systems with adaptive step size”, Journal of Automation, Mobile Robotics and Intelligent Systems, **18**, *3*, pp. 55–60 (2024).
7. H. Belmadani et al., “A new fast and efficient MPPT algorithm for partially shaded PV systems using a hyperbolic slime mould algorithm”, International Journal of Energy Research, **48**, *1*, pp. 1–10 (2024).
8. N. Ghanemi, D. Labed, “Optimal power flow solution of hybrid AC–DC network using particle swarm method”, Periodica Polytechnica

Electrical Engineering and Computer Science, **69**, *2*, pp. 137–147 (2025).
9. J. Águila León, C. Vargas Salgado et al., “Optimizing photovoltaic systems: a meta-optimization approach with GWO-enhanced PSO algorithm for improving MPPT controllers”, Renewable Energy, **230**, Article 120892 (2024).
10. H. Zheng, Q. Du et al., “Improved marine predator MPPT algorithm for photovoltaic systems in partial shading conditions”, Scientific Reports, **15**, *1*, Article 21092 (2025).
11. M.A.B Siddique, et al., “Performance validation of global MPPT for efficient power tracking through PV system under complex partial shading effects”, Scientific Reports, **15**, *1*, Article 17061 (2025).
12. D. Darjat, S.A. Bima, H.E. Evangelista, B. Winardi, A.A. Zahra, N.M. Tahir, “Hardware design for maximum power point tracking (MPPT) based on metaheuristic algorithm in photovoltaic (PV) systems”, Eastern European Journal of Enterprise Technologies, **6**, *5*, pp. 22–32 (2024).
13. A. Ammar, K. Hamraoui, M. Belguellaoui, A. Kheldoun, “Performance enhancement of PV water pumping system based on BLDC motor under partial shading condition”, Engineering Proceedings, **14**, Article 22 (2022).
14. S. Balakumar, M. Lemma, M. Godato, “Solar-powered ANN-based MPPT with zeta converter for BLDC motor water pump in rural Ethiopia for sustainable agriculture”, Discover Sustainability, **6**, *1*, p. 140 (2025).
15. M. Bouksaim, M. Mekhfioui, M.N. Srifi, “A comprehensive decade-long review of advanced MPPT algorithms for enhanced photovoltaic efficiency”, Solar, **5**, *3*, p. 44 (2025).
16. P. Priya, A.A. Stonier, “Advancements in maximum power point tracking (MPPT) techniques for solar photovoltaic (PV) applications: A comprehensive review”, Energy Conversion and Management X, **29**, p. 101438 (2026).
17. Y. Bouteraa, M. Khishe, “Dynamic Lévy–Brownian marine predator algorithm for photovoltaic model parameters optimization”, Scientific Reports, **14**, Article 29261 (2024).
18. E. Philibus, A.M. Zain, D.D. Prasetya et al., “Marine predator algorithm and related variants: a systematic review”, International Journal of Advanced Computer Science and Applications, **16**, *1*, pp. 544–568 (2025).
19. M.A. Soliman, H.M. Hasanien, A. Alkuhayli, “Marine predators' algorithm for parameter identification of triple-diode models”, IEEE Access, **8**, pp. 832–842 (2020).
20. M.I. Abdelwanis, A. Zaky, “Maximum power point tracking in a perovskite solar pumping system with a six-phase induction motor”, Rev. Roum. Sci. Techn. – Électrotechn. et Énerg., **69**, *1*, pp. 15–20 (2024).
21. F. Berttahar, S. Abdeddaim, A. Betka, O. Charrouf, “A comparative study of PSO, GWO, and HOA algorithms for maximum power point tracking in partially shaded photovoltaic systems”, Power Electronics and Drives, **9**, *1*, pp. 86–105 (2024).
22. M.Q. Taha, M.K. Mohammed, B. El Haiba, “Metaheuristic optimization of maximum power point tracking in PV array under partial shading”, Engineering, Technology & Applied Science Research, **14**, *3*, pp. 14628–14633 (2024).